Mon. Not. R. Astron. Soc. **356,** 1383–1395 (2005) doi:10.1111/j.1365-2966.2004.08570.x

Methods for computing giant planet formation and evolution

O. G. Benvenuto[1,2★]† and A. Brunini[1,3★]‡

[1]*Facultad de Ciencias Astronómicas y Geofísicas, Universidad Nacional de La Plata, Paseo del Bosque S/N, (1900) La Plata, Argentina*
[2]*Departamento de Astronomía y Astrofísica, Pontificia Universidad Católica, Vicuña Mackenna 4860, Casilla 306, Santiago, Chile*
[3]*Instituto Astrofisico de La Plata, Paseo del bosque s/n (1990) La Plata, Argentina*

Accepted 2004 October 29. Received 2004 October 29; in original form 2004 March 31

ABSTRACT

We present a numerical code for computing all stages of the formation and evolution of giant planets in the framework of the core instability mechanism. This code is a non-trivial adaption of the stellar binary evolution code and is based on a standard Henyey technique. To investigate the performance of this code we applied it to the computation of the formation and evolution of a Jupiter mass object from a half Earth core mass to ages in excess of the age of the Universe.

We also present a new smoothed linear interpolation algorithm devised especially for the purpose of circumventing some problems found when some physical data (e.g. opacities, equation of state, etc.) are introduced into an implicit algorithm like the one employed in this work.

Key words: planets and satellites: formation – galaxies: evolution.

1 INTRODUCTION

For many years, the only known gas giant planets were the four ones in our own Solar system. They provided unique observational evidence for theories of giant planet formation and evolution. However, this situation has changed drastically over the past decade with the discovery of more than 100 planets orbiting around main-sequence stars (see, for example, the web site http://www.obspm.fr/planets), revealing that gas giant planets are very common, at least in the solar neighborhood.

It is commonly assumed that gaseous giant planets have been formed by the core instability mechanism (Mizuno 1980), which states that a solid core is formed from the accretion of planetesimals in the protoplanetary disc, followed by the capture of a massive envelope from the gaseous component of the protoplanetary nebula. The whole process may be divided into some characteristic stages as follows.

(i) The accretion of solid planetesimals results in the growth of a solid core with several Earth masses. This solid core is surrounded by a tenuous gaseous envelope of very low mass.

(ii) As the solid core grows, gas is accreted at an increasing rate. At some time, the gas accretion rate supersedes the solid accretion rate.

(iii) When the mass of the envelope is comparable to the mass of the solid core, runaway gas accretion starts. During this stage, owing to the exhaustion of solids in the feeding zone of the planet, very little accretion of planetesimals occurs.

(iv) The accretion of gas is terminated, owing to dissipation or tidal truncation of the nebula.

(v) The planet cools and contracts at constant mass to its present state.

The characteristic time-scales involved in the various stages described above are very different. Steps (i) and (ii) can last for some millions of years, but during the runaway gas accretion, a gas giant can accrete one Jupiter mass of gas over a few 10^3 yr. During this stage, luminosity can rise to 10^{-3}–$10^{-4}\,L_\odot$ (Bodenheimer & Pollack 1986), in part owing to the release of gravitational energy forced by the violent initial contraction of the envelope, during the initial moments after the termination of the accretion process.

Although the core instability model is conceptually very simple, modelling it accurately is, to the contrary, difficult, and usually, some particular simplifying assumptions, for each one of the different stages, have to be adopted (Bodenheimer, Hubickyj & Lissauer 2000).

At present, very few codes capable of modelling the formation of giant planets, incorporating the relevant physics involved in the core instability model, exist. We can mention here the ones developed by Bodenheimer & Pollack (1986) (with many further improvements), and by Wuchterl (1990).

It is the aim of the present work to describe a numerical code for computing the formation and evolution of giant planets in the framework of the core instability model. This code is capable of computing all the formation stages, the subsequent detachment from the protoplanetary nebula and its final contraction and cooling. This code is a non-trivial adaption of a Henyey code tailored for computing stellar

★E-mail: obenvenuto@fcaglp.fcaglp.unlp.edu.ar; obenvenu@astro.puc.cl (OGB); abrunini@fcaglp.unlp.edu.ar (AB)
†Member of the Carrera del Investigador Científico, Comisión de Investigaciones Científicas de la Provincia de Buenos Aires, Argentina.
‡Member of the Carrera del Investigador Científico, Consejo Nacional de Investigaciónes Cientí ficas y Técnicas, Argentina.

evolution in close binary systems with mass transfer (Benvenuto & De Vito 2003).

This paper is organized as follows: in Section 2 we describe the main features of our code. In Section 3 we briefly describe the physical ingredients we have incorporated in our code. In Section 4 we show the performance of the code applying it to the formation and evolution of a Jupiter mass object from a half Earth core mass to ages in excess of the age of the Universe. Finally, Section 5 is devoted to our conclusions. We also present in the Appendix a new smoothed linear interpolation algorithm devised especially for circumventing some problems found when some tabulated data [e.g. opacities, equation of state (EOS), etc.] are introduced in an implicit algorithm like the one employed in our code.

2 THE EQUATIONS OF GIANT PLANET FORMATION AND EVOLUTION

2.1 Equations of structure and evolution

Here, we shall briefly summarize the equations of giant planet formation and evolution to be solved by our code. As usual, we consider spherically symmetric objects, neglecting rotation and magnetic fields. Despite the fact that it is currently accepted that giant planet formation and evolution is a phenomenon that occurs in conditions very near to those of hydrostatic equilibrium, we prefer to develop a full hydro code. Obviously, this is more general than an hydrostatic code. Moreover, it may happen that some planets are formed in conditions very different to those currently accepted for which hydrodynamic phenomena may be relevant.

In the conditions we are interested in, the equations of giant planet formation and evolution are as follows.[1]

(i) The Euler equation of fluid motion

$$\frac{1}{4\pi r^2}\frac{\mathrm{d}v}{\mathrm{d}t} = -\frac{\partial P}{\partial m_r} - \frac{G\,m_r}{4\pi r^4}. \tag{1}$$

(ii) The definition of velocity

$$\frac{\partial r}{\partial t} = v. \tag{2}$$

(iii) The equation of mass conservation

$$\frac{\partial r}{\partial m_r} = \frac{1}{4\pi r^2 \rho}. \tag{3}$$

(iv) The equation of energy balance

$$\frac{\partial l_r}{\partial m_r} = \varepsilon_{pl} - T\frac{\partial S}{\partial t}. \tag{4}$$

(v) The equation of energy transport for the radiative case

$$\frac{\partial T}{\partial m_r} = -\frac{3}{64\pi ac}\kappa\frac{l_r}{T^3 r^4}. \tag{5}$$

and

(vi) The equation of energy transport for the convective case

$$\frac{\partial \ln T}{\partial m_r} = \nabla_{\mathrm{conv}}\frac{\partial \ln P}{\partial m_r}, \tag{6}$$

where ∇_{conv} is the convective temperature gradient, which may be computed employing the standard mixing length theory (see, e.g. Kippenhahn & Weigert 1990).

[1] For the derivation of these equations see, e.g. Clayton 1968; Kippenhahn & Weigert 1990. For a detailed treatment of hydrodynamic stellar codes, see Kutter & Sparks 1972.

We consider the entropy differential in the form

$$T\,\mathrm{d}S = C_P\,\mathrm{d}T - \frac{\delta}{\rho}\,\mathrm{d}P \tag{7}$$

and we employ the Schwartzchild criterion for the onset of convection.

The total gravitational energy release owing to the accretion of planetesimals L_{pl} is given by

$$L_{\mathrm{pl}} = \frac{G M_{\mathrm{core}}\dot{M}_{\mathrm{core}}}{R_{\mathrm{core}}}. \tag{8}$$

We should remark that the planetesimal core accretion rate $\dot{M}_{\mathrm{core}}$ is not specified by these equations and remains an input of the model, not only in its initial value but also as regards its temporal variation. To incorporate this energy release we introduce the rate of planetesimal energy release $\varepsilon_{\mathrm{pl}}$ imposing the condition that

$$L_{\mathrm{pl}} = \int_{M_{\mathrm{core}}}^{M} \varepsilon_{\mathrm{pl}}\,\mathrm{d}m_r. \tag{9}$$

We have found it convenient to adopt an expression for $\varepsilon_{\mathrm{pl}}$ in a way that the energy release is produced near the bottom of the gaseous envelope as

$$\varepsilon_{\mathrm{pl}} = A\left(\alpha - \frac{m_r - M_{\mathrm{core}}}{M_{\mathrm{core}}}\right)^2. \tag{10}$$

$\varepsilon_{\mathrm{pl}}$ vanishes at $m_{\mathrm{env}} = \alpha\, M_{\mathrm{core}}$ (where $m_{\mathrm{env}} = m_r - M_{\mathrm{core}}$) and is set to zero outward. A is a constant determined by the conditions given by equation (9)

$$A = \frac{2}{\alpha(2+\alpha)}\frac{G\dot{M}_{\mathrm{core}}}{R_{\mathrm{core}}}. \tag{11}$$

While the results are fairly insensible to the precise value of the parameter α, we shall set $\alpha = 2$.

δ is given by

$$\delta = \left.\frac{\partial \ln \rho}{\partial \ln T}\right|_P \tag{12}$$

and the rest of the symbols have their standard meaning.

In dealing with the specific problem of giant planets we have to make some supplementary assumptions apart from those quoted previously. We shall handle the members of our system as spherical objects, neglecting the departure from spherical symmetry of the equipotentials (e.g. the pear-like shape of the Roche Lobe) and its evolutionary consequences. Moreover, we shall assume that a giant planet moves along a circular orbit.

As usual we shall describe the problem in Lagrangian coordinates. We shall consider the independent variable ξ, defined as

$$\xi = \ln\left(\frac{m_r}{M_{\mathrm{core}}} - 1\right). \tag{13}$$

In the calculations to be presented in Section 4, the mass of the core of the starting model is of the order of $M_{\mathrm{core}} = 0.6\,M_\oplus$ while the amount of gas gravitationally bound is $M_{\mathrm{env}} \sim 10^{-5}\,M_\oplus$. Meanwhile, models of evolved planets have $M_{\mathrm{core}} \sim 20\,M_\oplus$ while M_{env} may be as large as $M_{\mathrm{env}} \sim 3\times 10^3\,M_\oplus$. Thus, if we want to consider an interval in ξ on which we can accommodate all this evolution we need to take, say, $-16 \leqslant \xi \leqslant 10$ (see below).

As stated already, we are interested in computing the evolution of the gaseous part of the planet. In handling the core we shall simply assume it to have a constant density and neglect any processes that may release energy (e.g. radioactivity). However, this may be

included with some minor modifications in the strategy described here. In addition, the rate of core growth is an input of the model, at least in the present work (see Pollack et al. 1996 for a detailed treatment of the core growth rate).

We found it very convenient to handle radii, pressure and temperature by means of logarithmic transformations

$$p = \ln P,$$

$$\theta = \ln T,$$

$$x = \ln r,$$

whereas l_r, v are considered linearly.

For simplicity, we have written the difference equations in a centred fashion. This means that we have chosen to write a generic differential equation

$$\frac{\mathrm{d}y_i}{\mathrm{d}x} = F(x, y_1, \ldots, y_5); \quad i = 1, \ldots, 5 \tag{14}$$

as a difference equation

$$\frac{y_{i,j+1} - y_{i,j}}{x_{j+1} - x_j} - F(x_{j+1/2}, y_{1,j+1/2}, \ldots, y_{5,j+1/2}), \tag{15}$$

where $\eta_{j+1/2} = (\eta_{j+1} + \eta_j)/2$ with η being any quantity. The second subindex j indicates the shell of the star for which the difference equation is written. Temporal derivatives have been written in the standard backward differenced form.

With employing this recipe, for example, equation (3) becomes

$$\frac{x_{j+1} - x_j}{\xi_{j+1} - \xi_j} = \frac{M_{\rm core}}{4\pi} \frac{\exp(\xi_{j+1/2} - 3x_{j+1/2})}{\rho_{j+1/2}}. \tag{16}$$

Owing to its definition, ξ is *not* a time-independent coordinate. Thus, to write the equations taking this fact into account it is very useful to rewrite the derivative operator as

$$\left.\frac{\partial}{\partial t}\right|_{m_{\rm env}} = \left.\frac{\partial}{\partial t}\right|_{\xi} + \left.\frac{\partial \xi}{\partial t}\right|_{m_{\rm env}} \left.\frac{\partial}{\partial \xi}\right|_{t}. \tag{17}$$

Then, straightforwardly,

$$\left.\frac{\partial \xi}{\partial t}\right|_{m_{\rm env}} = -\frac{\mathrm{d}}{\mathrm{d}t} \ln M_{\rm core}. \tag{18}$$

To solve the problem we need to define some adequate boundary conditions.

2.2 Inner boundary conditions

We shall assume that the high-density core has a constant density $\rho_{\rm core}$ which we have fixed at a value of $\rho_{\rm core} = 3\,\mathrm{g\,cm^{-3}}$. Furthermore, we have neglected any energy release coming from the core apart from the one owing to its growth by the accretion of planetesimals. Thus, in this case, the inner boundary conditions to be applied at the bottom of the envelope (where $M_r = M_{\rm core}$) are given by

$$M_{\rm core} = \frac{4}{3}\pi \rho_{\rm core} R_{\rm core}^3 \tag{19}$$

and

$$L_r(m_r = M_{\rm core}) = 0. \tag{20}$$

Finally, the inner boundary condition for velocity is given by core growth which is

$$v(m_r = M_{\rm core}) = \frac{\dot{M}_{\rm core}}{4\pi R_{\rm core}^2 \rho_{\rm core}}. \tag{21}$$

2.3 Outer boundary conditions

2.3.1 The formation stage

In the formation stage, as usual, we shall consider the external radius of the planet R as the minimum of the accretion radius $R_{\rm acc}$ and the Hill radius $R_{\rm Hill}$ defined as

$$R_{\rm acc} = \frac{GM}{c^2} \tag{22}$$

(where c is the local velocity of sound) and

$$R_{\rm Hill} = a\left(\frac{M}{3M_{\rm star}}\right)^{1/3}. \tag{23}$$

The planetary radius thus is

$$R = \min[R_{\rm acc}, R_{\rm Hill}], \tag{24}$$

respectively. Physically, the accretion radius is the place at which the molecular velocity equals the escape velocity, while the Hill radius corresponds to the equivalent radius of a sphere with a volume equal to that of the Roche lobe of the planet.

Usually, it has been considered that at R the temperature and density of the planet corresponds to those of the protoplanetary nebula denoted as $T_{\rm neb}$ and $\rho_{\rm neb}$, respectively. From a numerical point of view we have found it very convenient to impose the boundary conditions in a different way. Let us consider, as discussed earlier, the possibility of extending the grid far beyond the planetary edge. If we introduce some kind of softening of the gravitational potential owing to the presence of a limiting physical agent, this softening makes the gradient of the gravitational potential drop to zero near the planetary radius and thus, we shall have, apart from the hydrodynamical effects, a constant pressure. But, as the gradient of temperature is proportional to the pressure gradient, we shall also have a constant temperature region. Consequently, the density in such a region will have also a flat profile. In these conditions we can impose the physical boundary conditions corresponding to the planetary surface at the outermost point of the grid chosen to be located far outside the planet. In other words, handling the outer boundary conditions in the way described above we set $T = T_{\rm neb}$ and $P = P_{\rm neb}$ for a value of the independent coordinate $\xi = \xi_{\rm edge}$ far larger than that corresponding to the planet. For an adequate softening of the gravitational potential we shall have $T = T_{\rm neb}$ and $P = P_{\rm neb}$ for values of ξ from $\xi_{\rm edge}$ up to the value corresponding to the actual planetary surface $\xi_{\rm surf}$, where $\xi_{\rm surf} = \ln\,(M/M_{\rm core} - 1)$. When the planet begins to undergo a noticeable growth, R will increase. In accounting for this effect we only have to change the radius in the function adopted for the quoted softening, as the planetary boundary conditions will be automatically fulfilled.

Specifically, we have introduced a restricted three-body spherically averaged gravitational potential (which is the standard one), multiplied by the factor

$$1 - \left(\frac{r}{R}\right)^3. \tag{25}$$

We apply this factor up to a predetermined fraction of the planetary radius $r \leqslant \zeta\ R$. For larger values of r we have found it convenient to use a Fermi-like function

$$\left[1 + \exp\left(\frac{r - \zeta R}{\beta R}\right)\right]^{-1} \tag{26}$$

with continuity of the function and its first derivative being at the point $r = \zeta R$. This gives $A = 2\,(1 - \zeta^3)$ and $\beta = (1 - \zeta^3)/(6\zeta^2)$.

We have tested values of ζ in the range $\zeta = 0.90$–0.99 finding that the global properties of the evolution of the planet are fairly insensitive to the value of ζ. In addition, from a numerical point of view very good convergence is produced if we take care when defining a grid which is dense enough near $r = R$.

If we consider the strictly flat profiles for T and P at the interval $\xi_{\rm surf} \lesssim \xi \leqslant \xi_{\rm edge}$, this treatment will allow the planetary envelope to grow at rates which can be arbitrarily high (of course, the precise rate of growth of the planet will be the solution of the equations). However, if the protoplanetary nebula has a low-density gap near the planetary surface, this will naturally impose a upper limit for the gas accretion rate of the envelope. Preliminary calculations, which are beyond the scope of the present paper, indicate that the scheme we present here is adequate for considering migration, the occurrence of a gap in the gas distribution in the protoplanetary disc and also non-constant planetesimal core accretion rates.

2.3.2 *The evolution stage*

In handling the outer boundary conditions at the evolutionary stage we have to take into account the irradiation from the central star. This irradiation has a non-negligible effect on the evolution of the giant planet and should be especially important in the case of small planets at advanced evolutionary stages (like Saturn) or in the case of extrasolar giant planets orbiting very close to the central star (see Section 1).

Notice that irradiation has an obvious non-radial nature. However, to work in spherical symmetry form we shall consider that this energy is distributed uniformly over the whole surface of the planet. Otherwise we would be forced to change our whole treatment from the very beginning. Let us remark that in the case of the giant planets of our Solar system, rotation is very fast making the irradiation of the planetary surface approximately uniform. In more general conditions we should expect some kind of fluid circulation from the irradiated hemisphere to the opposite hemisphere to be driven by the presence of a temperature gradient. While this effect should be of fundamental relevance in computing the spectra of irradiated planets, it seems that assuming uniform irradiation is acceptable for our purposes.

In the framework of these approximations, we define $L_{\rm irr}$ as the fraction of the energy irradiated by the parent star absorbed by the illuminated hemisphere of the planet (see, e.g. Guillot 2001)

$$L_{\rm irr} = L_*(1 - A)\left(\frac{R}{2a}\right)^2. \tag{27}$$

Here L_* is the luminosity of the parent star and A is the Bond albedo of the planet.

With regards to the strategy for handling the integration of the outer layers, we shall introduce a method that represents a generalization from the one presented by Kippenhahn, Weigert & Hofmeister (1967) devised in the case of stellar evolution. They proposed to divide the $\log\ L - \log\ T_{\rm eff}$ (where L is the luminosity and $T_{\rm eff}$ is the effective temperature) plane into rectangle triangles, employing integration of the outer layers at the vertexes of a given triangle containing the point corresponding to the actual $\log\ L - \log\ T_{\rm eff}$ values of a given model. They compute integrations of the outer layer for the conditions at each vertex and apply the outer boundary conditions to the model by means of two-dimensional linear interpolation.

In stellar evolution, luminosity, effective temperature and radius are related by the well-known relation

$$L = 4\pi R^2 \sigma T_{\rm eff}^4, \tag{28}$$

in which all these quantities are positive. However, in the case of an irradiated planet we have (see, e.g. Guillot 2001)

$$L + L_{\rm irr} = 4\pi R^2 \sigma T_{\rm eff}^4, \tag{29}$$

where $L_{\rm irr}$ is given by equation (27). If we assume $L_{\rm irr}$ is constant, the planet would cool down asymptotically to an effective temperature $T_{\rm eff}\|_0$ given by

$$\mathrm{L_{irr}} = 4\pi R^2 \sigma \left(T_{\rm eff}\big|_0\right)4. \tag{30}$$

However, for most of the recently discovered extrasolar giant planets, the parent star is undergoing core hydrogen burning (the so-called main-sequence stage; see, e.g. Kippenhahn & Weigert 1990). In the main sequence, stars suffer from a increase in luminosity.[2] Consequently, even without migration, radiation increases as a function of time. Thus, it is possible to have a situation in which the planet reaches equilibrium at a finite age. From that moment on, as irradiation increases monotonically, the planet will begin to absorb energy from its parent star, i.e., L becomes *negative*. This situation does not happen in stellar evolution, and forces us to modify the strategy of Kippenhahn et al. (1967).

To maintain this kind of strategy we are forced to divide a plane defined by logarithmic axes (this is very convenient owing to the enormous variations in the outer conditions of the giant planets during their whole evolution). Thus, obviously, these axes must correspond to positively defined quantities. In the case of the evolution of a giant planet including irradiation from its parent star we shall divide the plane $\log\ R - \log\ T_{\rm eff}$ in to rectangle triangles. Assuming a value for the radius we immediately compute a value of $L_{\rm irr}$ (see equation 27), and then, by means of equation (29) we get the corresponding value of L. Thus, we are then able to perform integration of the standard outer layers using standard methods (e.g. Runge–Kutta).

In computing the structure of the outermost layers of the planet we have employed equations (1), (3), (5) and (6), neglecting terms containing temporal derivatives (which means that we have neglected the inertia and heat content of these layers). Consequently, these layers have a constant luminosity value. As in deeper layers, we have considered the fully non-ideal EOS (see Section 3), non-adiabatic convection and imposed the Schwartzchild criterion for the onset of convection.

As is usual in stellar evolution calculations, these layers are integrated taking the total pressure as the independent variable. Regarding the fraction of mass we include in these outer layers integrations, it is advisable to keep the amount of mass in the integration of the outer layers $M_{\rm OL}$ as small as possible to avoid neglecting significant gravitational energy release caused by contraction. In the case of our code we have assumed $M_{\rm OL}/M_{\rm planet} \lesssim 10^{-3}$.

2.3.3 *The in-between stage*

A non-trivial problem is the way in which a planet detaches from the protoplanetary nebula. In our code we have used the simplest hypothesis: when the object reaches a prefixed amount of gravitationally bounded matter we abruptly change the boundary conditions from those of the protoplanetary nebula to those described

[2] For example in the case of the Sun, its luminosity has increased by approximately 40 per cent since it ended its pre-main-sequence contraction.

in the previous sub-subsection corresponding to the evolutionary stage. Needless to say, this represents a gross oversimplification of the actual physical situation. This should be regarded as completely unsatisfactory in the case where we are particularly worried about the behaviour of the planet at the time when it is close to detachment. However, for the present work our main concern is to reach an accurate description of the whole behavior of the system. In this sense we consider that the current treatment suffices for our purposes in an initial approach to the problem.

As will be described next, the planet reaches a very short-lived high-luminosity stage which we interpret to be essentially unobservable. In addition, the maximum of the effective temperature of the planet is reached very soon after detachment from the protoplanetary nebula. A very important point to investigate is the dependence of the shape of the evolutionary track of the planet upon the way it detaches from the protoplanetary nebula employing more realistic models than the one assumed in this paper.

2.4 The overall problem

Taking into account all the details already described, we handle the equations in a fully implicit way by means of the Henyey technique as presented in Kippenhahn et al. (1967). We found very fast convergence of the code in most of the conditions being considered with the remarkable exception of the moment of detachment from the protoplanetary nebula.

3 THE PHYSICAL INGREDIENTS OF THE CODE

In the present version of the code we have incorporated the EOS presented by Saumon, Chabrier & van Horn (1995). This EOS has been especially devised for computing low-mass objects like brown dwarfs and giant planets. It represents a very detailed treatment for hydrogen plasma and another, less detailed, approach for helium.

While the treatment performed in computing the Saumon et al. (1995) EOS is detailed enough for the purposes of this work, we found some serious numerical problems in using it as part of an iterative scheme like the code presented in this paper. As is to be expected, the density of the plasma is a rather smooth function throughout the whole interval of temperatures and pressures, however, by contrast, quantities which represent second derivatives of free energies (e.g. C_P, ∇_{ad} and δ) are functions with steep variations.

For the formation stages and low temperatures we have considered grain opacities given by Semenov et al. (2003) in the case of low densities and by Pollack, McKay & Christofferson (1985) for higher densities. For the evolutionary stages we considered the opacity data given by Guillot (1999). For temperatures above 10^3 K we considered the molecular opacities of Alexander & Ferguson (1994), which are available up to $T \leqslant 10^4$ K and for higher temperatures we considered the opacities given by Rogers & Iglesias (1992). Notice, that at such conditions we expect the interiors of giant planets to be in convective equilibrium. Owing to this, radiative opacities are of little importance in such a regime.

These difficulties found in handling C_P, ∇_{ad} and δ are even more serious in the case of the opacities. This is especially so at very low temperatures where dust makes a large contribution.

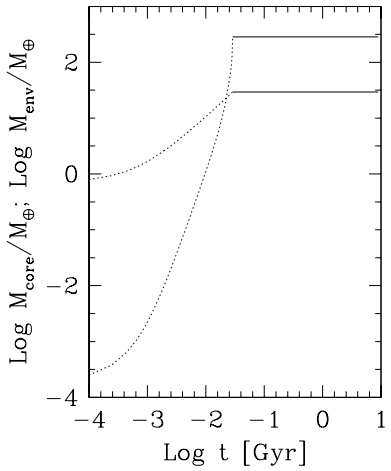

Figure 1. The logarithm of the masses of the core and gaseous envelope of the planet since the beginning of formation. Formation stages are displayed in dotted lines while evolutionary ones in solid lines. We considered the formation of the object up to the moment at which it was able to bound a mass of 1 $M_{\rm Jup}$. Since then on we considered constant mass evolution. We should remark that the mass of the core as a function of time is an input whereas the mass of the gaseous envelope is a solution of the structure and evolution equations (see Section 2). The starting model has a total mass of 0.6 $M_\oplus$ and a very tiny amount of bounded gas. As the core grows, about 20 Myr later the mass of the planet has undergone an appreciable growth and now half the total mass is in the core and the other in the gaseous envelope. From this moment on there runaway instability occurs and very soon the planet reaches its assumed final mass value.

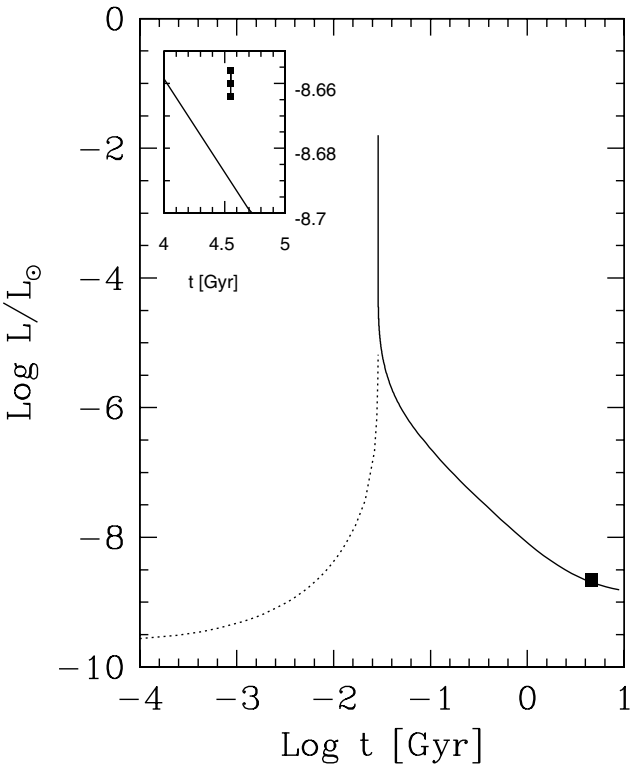

Figure 2. The luminosity of the planet as a function of time for the formation of an 1-$M_{\rm Jup}$ mass object. Here, the formation (dotted lines) and evolution stages (solid line) are clearly differentiated (see Fig. 1). Formation corresponds to the times before the runaway gas accretion instability, which corresponds to moments just before the flash-like luminosity peak. Detachment from the protoplanetary nebula is assumed to occur when the object has a total gravitationally bound mass of 1 $M_{\rm Jup}$. The evolutionary stages at constant mass correspond to moments after the luminosity flash. The filled square indicates the position of Jupiter, while in the inset we compare the computed luminosity of the Jupiter model at an age equal to that of the Solar system with the one observed with its corresponding error bar (notice that in the inset the horizontal scale is linear).

While the EOS is reasonably well established, it seems that this is not the case for opacities. In a recent work, Podolak (2003) re-examined the opacity owing to grains finding it to be significantly lower than earlier estimates. Remarkably, the values of the opacities are among the most important ingredients in determining the critical mass of the core for reaching core instability. Opacities that are lower than the ones considered here would produce lower critical core mass values which, in turn, would be formed faster thus alleviating the well-known problem of the time-scales of formation of giant planets in the framework of a core instability mechanism (see also Section 1).

In the near future we plan to incorporate a few very low energy nuclear reactions (particularly deuterium burning) experienced by very massive giant planets (with masses $M \gtrsim 14\,M_{\rm Jup}$; see, e.g. Burrows et al. 1995).

4 THE CASE OF A JUPITER MASS OBJECT

As an initial application of the code presented in the previous section, we shall present the results we have found employing the code corresponding to the formation of a Jupiter mass object of solar composition at a fixed orbit of 5.2 au. We should remind the reader that it is not our aim here to present a state-of-the-art model of the formation of Jupiter *but* to show the results the numerical scheme presented above is capable of producing. At this point we should remark that many of the characteristics of the solution we shall describe next are also present in previous calculations (see, e.g. Bodenheimer et al. 2000).

For simplicity, we shall assume a constant rate of accretion of planetesimals of $10^{-6} M_{\oplus}$ yr^{-1}, a constant density for the core $\rho_{\rm core} = 3$ g cm^{-3} and start with a model of 0.6 $M_{\oplus}$ which has attached a gravitationally bound gaseous envelope of $\approx 10^{-6}\,M_{\oplus}$. With regards to the physical conditions at the protoplanetary nebula, we shall assume that they remain constant with a density $\rho_{\rm neb} = 10^{-10}$ g cm^{-3} and temperature $T_{\rm neb} = 100$ K. In addition, we shall employ an adiabatic temperature gradient in the convective zones.

The computation comprised about 10 000 models resolved in about 2000 mesh points. The main characteristics of the numerical solution are presented in Figs 1–8 and Table 1. We shall include solar irradiation assuming a constant luminosity of 1 $L_{\odot}$.

In Fig. 1 we show the mass of the core and the total planetary mass as a function of time. Notice that the final growth of the gaseous envelope occurs in a fairly short time-scale as expected with the core instability mechanism.

In Fig. 2 we show the luminosity of the planet as a function of time. Notice that there exists a very sharp peak in the luminosity owing to gravitational energy release driven by the violent contraction of the outermost layers of the gaseous envelope. Prior to that, luminosity was rather proportional to $t^{2/3}$ because we assumed a constant core growth rate. After the peak, luminosity decays nearly exponentially

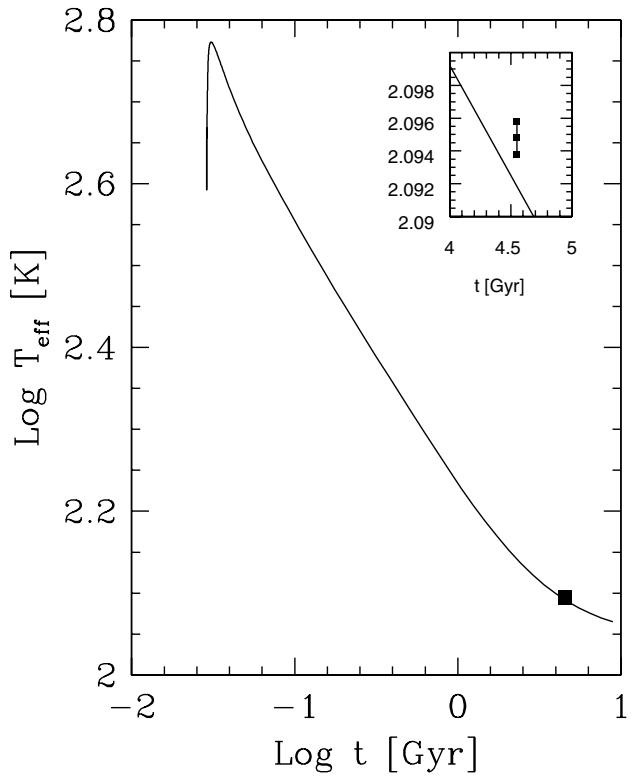

Figure 3. The effective temperature of the planet as a function of time for the formation of an 1-$M_{\rm Jup}$ mass object. Here we have only considered the evolutionary stages. Notice that the maximum of the effective temperature occurs just after detachment from the nebula (see Table 1). The filled square indicates the position of Jupiter, while in the inset we compare the computed effective temperature of the Jupiter model at an age equal to that of the Solar system with the observed one with its corresponding error bar (notice that in the inset the horizontal scale is linear).

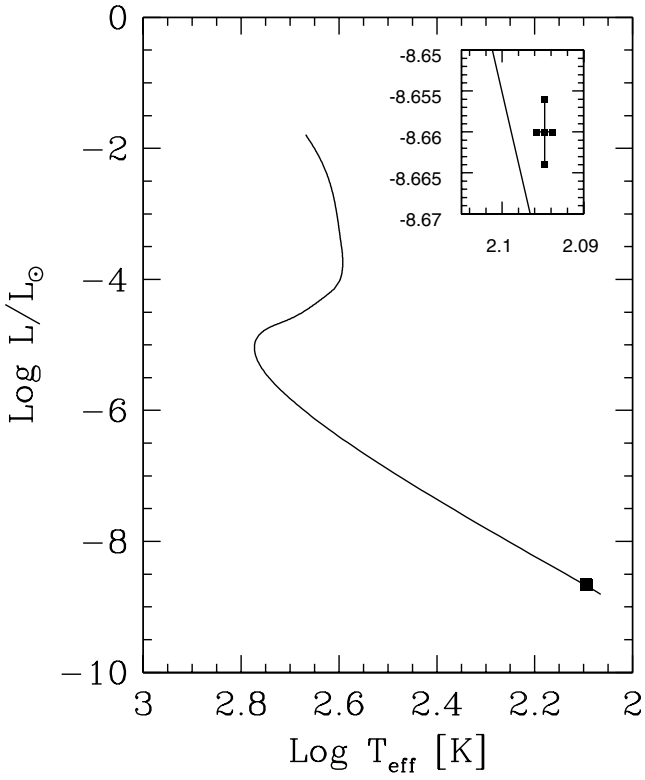

Figure 4. The evolutionary track of the 1-$M_{\rm Jup}$ mass object since detachment from the protoplanetary nebula. Soon after detachment the planet undergoes fast contraction and reaches the maximum effective temperature almost immediately. The planet then reaches its final cooling track. This evolution occurs approximately at constant radius as to be expected for a semidegenerate object. The filled square indicates the position of Jupiter, while in the inset we compare the computed evolutionary track of the Jupiter model with the position of the present Jupiter with its corresponding error bars.

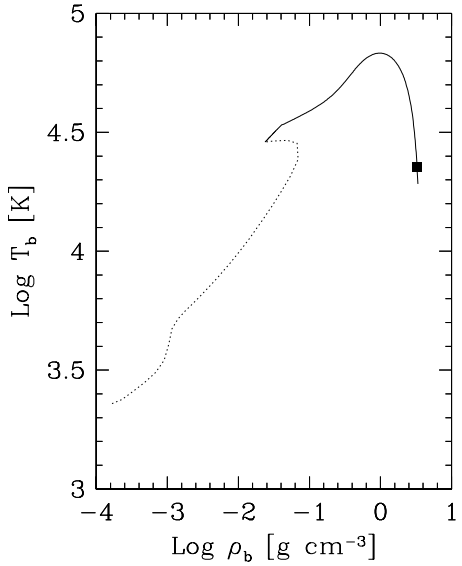

Figure 5. The evolution of the bottom of the gaseous envelope of a 1-$M_{\rm Jup}$ planet the formation (dashed line) and subsequent evolution (solid line). Temperature and density increase monotonically up to the start of the runaway growth of the envelope. As a consequence of the end of the formation stage, the bottom of the envelope begins to compress, reaching its maximum temperature (see Table 1). The conditions here computed for the present Jupiter are represented with a solid square.

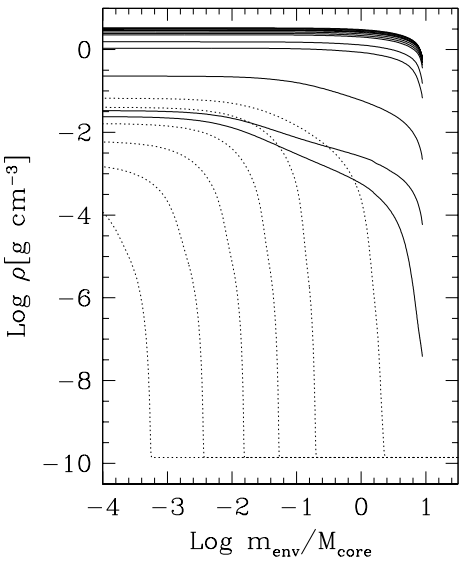

Figure 6. The evolution of the logarithm of density as a function of the transformed mass scale given by equation (13). We represent the profiles of the formation (evolution) models in dashed (solid) lines. Here, the included models correspond to those whose main characteristics are given in Table 1. Initially, the formation models have a very tiny amount of matter attached to the solid core and, consequently, the fall of density from the conditions at the bottom of the envelope to those in the protoplanetary nebula occur in a very narrow mass interval. As the core grows, the density profile becomes less steep. This is especially so at the runaway conditions. When the object detaches from the protoplanetary nebula it undergoes a global monotonic contraction up to the final computed model. In the profiles corresponding to the evolution stage, we have not included the part corresponding to the integrations of the outermost layers ($\approx 10^{-4} M_{\rm Jup}$).

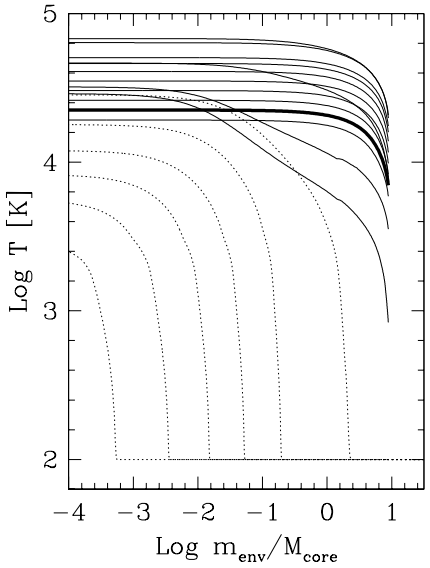

Figure 7. The evolution of the logarithm of the temperature as a function of the transformed mass scale given by equation (13). We have included the same models as in Fig. 6 and the lines have the same meaning as there. Notice the strong resemblance between the temperature profiles and the density ones (see Fig. 6). This is owing to the fact that during the whole formation stage, the EOS of the gas is essentially that corresponding to a ideal, non-degenerate gas. An important difference occurs at the final computed stages. Owing to the global cooling of the planet, the final plotted profile is cooler than the previous one. Here we have also excluded integrations of the outer layer from the figure while the heavy line corresponds to the conditions computed for the present Jupiter.

up to the moment where solar irradiation becomes important. At these advanced stages cooling noticeably slows down.

In Fig. 3 we depict the effective temperature of the planet as a function of time. In this figure we have only included the evolutionary stages in which a physically plausible effective temperature can be defined (see equation 29). Remarkably, the maximum in the effective temperature is reached almost immediately after detachment from the nebula.

In Fig. 4 we show the evolutionary track of the model. After detachment the object begins to evolve to higher effective temperatures and lower luminosities. After the maximum effective temperature it begins to cool down approximately on a constant radius track. Qualitatively, this part of the track resembles one corresponding to a very low mass white dwarf star. This is to be expected for a an object with a semidegenerate interior.

Fig. 5 describes the evolution of the bottom of the gaseous envelope of the planet. During formation the temperature and density increase monotonically up the beginning of the runaway growth of the envelope. Under these conditions, the bottom of the envelope reaches maximum density and decompresses at an approximately constant temperature. As a consequence of the formation stage finishing, the bottom of the envelope begin to compress, reaching a maximum temperature of 6.8×10^3 K at an age of 32.4 Myr. Notice that the maximum temperature reached by the planet is far lower than that needed for deuterium burning.

In Figs 6–7 we show the profiles of density and temperature for the formation and evolution stages of the planet. Notice that for most of the stages included in these plots, the profiles are very similar in each figure. This is because at formation stages the densities attained at the planetary interior are so low that any non-ideal effects

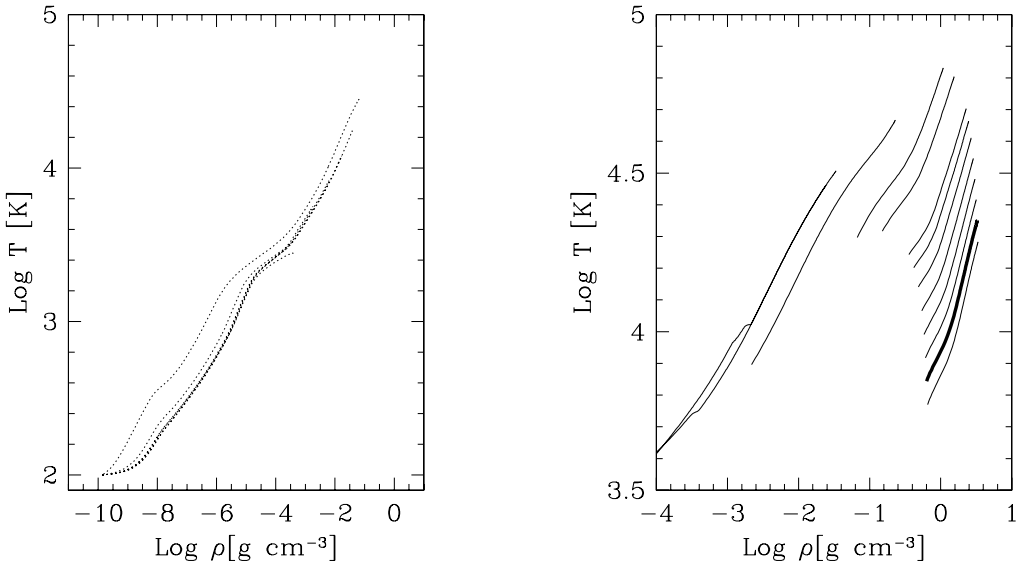

Figure 8. The evolution of the temperature–density profiles during formation (left panel) and evolution (right panel) for the same models as in Figs 6–7. In the evolution panel we have excluded the integrations of the outer layers from the figure. Notice that all profiles corresponding to the formation stage begin at the same point corresponding to protoplanetary nebula conditions $\rho_{\rm neb} - T_{\rm neb}$. During formation the curves evolve upwards while at the evolutionary stages they evolve to higher densities. The heavy line in the right panel corresponds to conditions computed for the present Jupiter.

Table 1. Selected stages of formation of a 1-$M_{\rm Jup}$ planet at 5.2 au from a 1-$M_\odot$ central star. Stages at which we do not give a value for the effective temperature corresponding to formation stages while the others denote evolutionary stages.

Age (Myr)	$\log L/L_\odot$	$\log T_{\rm eff}$ (K)	$\log T_{\rm b}$ (K)	$\log \rho_b$ (g cm^{-3})	$M_{\rm core}/M_\oplus$	$M_{\rm env}/M_\oplus$
0.43	−9.45224	···	3.44819	−3.31953	1.12723	0.00064
1.89	−9.17959	···	3.74837	−2.75196	2.58029	0.00961
3.98	−8.92438	···	3.91683	−2.21119	4.66760	0.07308
7.31	−8.60192	···	4.07892	−1.78309	8.00704	0.43547
13.44	−8.09241	···	4.25318	−1.39259	14.1356	2.86654
26.33	−6.67421	···	4.45348	−1.17511	27.0223	64.1232
28.75	−1.79705	2.67002	4.46112	−1.61632	29.4446	283.662
28.76	−3.96061	2.59590	4.50658	−1.47310	29.4446	283.662
29.06	−4.58208	2.69400	4.66691	−0.63959	29.4446	283.662
33.60	−5.36100	2.75742	4.83144	0.035113	29.4446	283.662
43.44	−5.84009	2.69707	4.80376	0.189012	29.4446	283.662
115.49	−6.73943	2.53285	4.70313	0.358696	29.4446	283.662
176.30	−7.03552	2.47065	4.66380	0.393792	29.4446	283.662
316.92	−7.41087	2.38840	4.61022	0.428709	29.4446	283.662
629.52	−7.82061	2.29533	4.54606	0.459719	29.4446	283.662
1238.99	−8.19652	2.20771	4.48137	0.482887	29.4446	283.662
2428.41	−8.49799	2.13681	4.41615	0.500708	29.4446	283.662
4693.17	−8.69854	2.08993	4.35056	0.514520	29.4446	283.662
8897.95	−8.80842	2.06494	4.28330	0.525822	29.4446	283.662

are of minor relevance. So, the EOS is well accounted for by a simple ideal, non-degenerate EOS. Notice, however, an important difference: while the density profiles evolve to higher values in most of the evolutionary stages, temperature profiles do not. This is so at the final evolutionary stages of the object at which it undergoes global cooling. We also show, in Fig. 8 the evolution of the gaseous envelope in the thermodynamic plane. Finally, for completeness, in Fig. 9 we show the evolution of the radii of the spheres containing a fixed amount of mass.

We should remark that, in spite of the fact that in this computation we did not set an upper limit to the growth of the envelope mass $\dot{M}_{\rm env}$ (see Section 2.3.1 for a discussion), we found it has been $\dot{M}_{\rm env} \leqslant 10^{-3}\, M_\oplus\ {\rm yr}^{-1}$ even during runaway growth.

To compare with the observational data corresponding to the present characteristics of Jupiter, we should note that at the present age of the Solar system (4.55×10^9 yr), the luminosity of Jupiter is $\log\ L_{\rm Jup}/L_\odot = -8.660 \pm 0.004$ while its effective temperature is $\log\ (T_{\rm eff})_{\rm Jup} = 2.0948 \pm 0.001$ (Pearl & Conrath 1991). In these data the reflected light is *not* included. In Figs 2–4 we have included insets in which we included the corresponding computed evolutionary curve together with the observations with error bars. We notice that at the age of the Solar system the Jupiter model is slightly

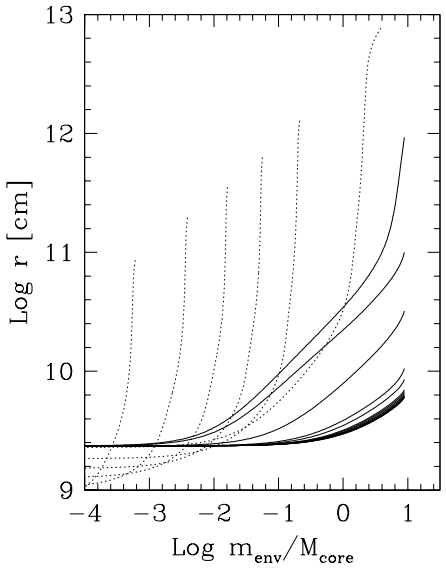

Figure 9. The evolution of the radius profiles of the models as a function of total mass for the same models included in Figs 6 and 7.

smaller than the real planet. While the effective temperature shows good agreement with the observations, the model reveals itself as somewhat underluminous. We consider these results as satisfactory taking into account the simplifying assumptions we made in this computation.

5 CONCLUSIONS

The goal of this paper has been to present a numerical code intended for computing all stages of the formation and evolution of giant planets in the framework of the core instability mechanism. This code is based on the standard Henyey technique usually employed in stellar evolution calculations.

Perhaps the key point of this method is the kind of change of variables given in equation (13), particularly considering the total mass in units of the core mass. If we naively choose a more straightforward independent variable like, for example, total mass, we would encounter serious trouble when computing the temporal derivative of entropy during the formation stages. With this kind of natural coordinate we would have an outwards migration of the envelope. Thus, to compute the difference in entropy between consecutive models at the same envelope mass element we would be forced to introduce some interpolations. But interpolations introduce numerical noise. This noise may be irrelevant at some stages but it is catastrophic during runaway growth and would prevent its calculation.

In testing the code we computed the formation and evolution of a Jupiter mass object from a 0.6 $M_\oplus$ core mass to ages in excess of the age of the Universe. While this should not be considered a state-of-the-art calculation (owing to the many simplifying assumptions, see Section 4), it shows that the general structure of the code works fairly well in simulating the whole process of the formation and evolution of giant planets.

We also present a new smoothed linear interpolation algorithm devised especially to circumvent some of the problems we found when introducing physical data into an implicit algorithm like the one employed in this work. This has been very important in allowing us to incorporate the detailed physics of the problem. These ingredients have some dramatic discontinuities owing to very important physical reasons (in opacities the grain evaporation and in the EOS the plasma phase transition). While the motivation in developing the method has been very specific, in our opinion it may be a valuable method for interpolating in more general conditions.

ACKNOWLEDGMENTS

We want to thank the anonymous referee for his/her constructive criticism that enabled us to greatly improve the original version of the present work. OGB was partly supported by the project FONDAP 15010003. AB acknowledges the financial support of AGNPCyT, PICT 03-11044.

REFERENCES

Alexander D. R., Ferguson J. W., 1994, ApJ, 437, 879
Akima H., 1970, J. ACM, 17, 589
Benvenuto O. G., De Vito M. A., 2003, MNRAS, 342, 50
Bodenheimer P., Pollack J. B., 1986, Icarus, 67, 391
Bodenheimer P., Hubickyj O., Lissauer J. J., 2000, Icarus, 143, 2
Burrows A., Saumon D., Guillot T., Hubbard W. B., Lunine J. I., 1995, Nat, 375, 299
Clayton D. D., 1968, Principles of Stellar Evolution and Nucleosynthesis. Mc Graw Hill, New York, p. 612
Dorfi E. A., 1997, in Steiner O., Gautschy A., eds, Computational Methods for Astrophysical Fluid Flow. Springer Verlag, Berlin, p. 263
Duff G. F., Naylor D., 1966, Differential Equations of Applied Mathematics. J. Wiley & Sons Inc., New York, p. 346
Gradshteyn I. S., Ryzhik I. M., 1994. Table of Integrals, Series and Products. Academic Press, New York, p. 1204
Guillot T., 1999, Plan. Space Sci., 47, 1183
Guillot T., 2001, 31th Saas-Fee Advanced Course on Brown Dwarfs and Planets, in press
Guillot T., Chabrier G., Morel P., Gautier D., 1994, Icarus, 112, 337
Kippenhahn R., Weigert A., Hofmeister E., 1967, Meth. Comp. Phys., 7, 129
Kippenhahn R., Weigert A., 1990, Stellar Structure and Evolution. Springer-Verlag, Berlin, p. 486
Kutter G. S., Sparks W. M., 1972, ApJ, 175, 407
Mizuno H., 1980, Prog. Theor. Phis., 64, 544
Pearl J. C., Conrath B. J., 1991, J. Geophys. Res. Journal, 96, 18921
Podolak M., 2003, Icarus, 165, 428
Pollack J. B., McKay C. P., Christofferson B. M., 1985, Icarus, 64, 471
Pollack J. B., Hubickyj O., Bodenheimer P., Lissauer J. J., Podolak M., Greenzweig Y., 1996, Icarus, 124, 62
Press W. H., Teukolsky S. A., Flannery B. P., Vetterling W. T., 1992, Numerical Recipes. Cambridge Univ. Press, Cambridge, p. 963
Rogers F. J., Iglesias C. A., 1992, ApJ, 401, 361
Saumon D., Chabrier G., van Horn H. M., 1995, ApJS, 99, 713
Semenov D., Henning T., Helling C., Ilgner M., Sedlmayr E., 2003, A&A, 410, 611
Wuchterl G., 1990, A&A, 238, 83

APPENDIX A: SMOOTHED LINEAR INTERPOLATION ALGORITHM

In this Appendix we shall describe an algorithm we have developed in order to overcome some of the delicate numerical problems we have had in preparing our code for planetary formation and evolution. In spite of the very specific motivation in constructing this interpolation method, this is very general and may be interesting for other applications. Because of this reason, hereon we shall describe it in detail.

In many numerical simulations of astrophysical interest, it is very common to have to interpolate tabulated data, representing some

physical quantity. Usually, these quantities are computed by means of complex numerical procedures. Even if the codes that produce the tabulated data were available, using them as subroutines would be impractical and wasteful.

Good examples of such a case are found in Section 3 where physical quantities such as the EOS of the plasma, radiative opacities, etc., in planetary interiors must be obtained as a function of pressure (or density) and temperature from a given table. Although these tables are dense enough so as to provide good interpolated values, the numerical derivatives of many interpolation algorithms exhibit discontinuities which often make it difficult to find a numerical solution of the problem (i.e. in the case of implicit schemes like the one presented in this paper, the convergence of the iterative algorithms usually turns out to be cumbersome). Even if convergence is attained, smooth derivatives are needed to prevent any spurious oscillations around steep gradients (Dorfi 1997). Simple approximations such as cubic splines (Press et al. 1992) are unreliable, because they may exhibit strong oscillations between tabulated values. Such spurious oscillations may be even stronger in the derivative of the function inhibiting convergence of the main iterative loop.

In principle, there exists a large number of ways to accomplish such a task. One possibility is to employ rational spline interpolation or the interpolants of Akima (1970). In this Appendix we shall present an alternative method for representing tabular data, which is not an interpolation but a kind of *'smooth representation'* and offers continuous, analytic derivatives. This method is very simple, being thus an alternative to be used in numerical simulations where the smoothness of the involved functions is of prime importance.

This Appendix will be organized as follows: in Section A1 we present the method and its main properties. Some specific weight functions are presented and studied in Section A2. Section A3 is devoted to the study of the effect of the smoothing here proposed for the spectrum of frequencies of the interpolation. In Section A4, some examples and comparisons with the most-standard procedures are displayed. The last section will be devoted to general comments on the properties of the method.

A1 The algorithm

Let us suppose that we have a table of values y_n, $n = 1, \ldots, N$ of the function $y(x)$, for given x_n, not necessarily evenly spaced. A simple way to interpolate a value of $y(x)$ for a non-tabulated x ($x_n < x < x_{n+1}$) is by means of linear interpolation

$$y_{\rm int}(x) = y_n + y'_n(x - x_n), \tag{A1}$$

where $y'_n = (y_{n+1} - y_n)/(x_{n+1} - x_n)$. The linear interpolation is continuous throughout the table but its numerical derivative is a step piecewise function, thus exhibiting discontinuities at the tabulated x_n values. Owing to the reasons detailed in Section A, such discontinuities in the derivative are highly undesirable. In what follows we shall present an algorithm specifically designed to avoid this problem in the framework of linear interpolations which can also be straightforwardly extended to interpolations of higher degrees.

The central idea of our algorithm is to represent the function $y(x)$ by means of appropriate weighting of the linear piecewise interpolated values $y_{\rm int}$ with a given weight function. This weight function must be chosen in order to assign high weights to values of $y_{\rm int}$ near the interpolation region, and considering with less relevance those values away from this point. With $\theta(x, x_n, x_{n+1})$ being the weight function, we define the representation of $y(x)$ as

$$y_\theta(x) = \sum_{n=1}^{N-1} y_{\rm int}(x)\,\theta(x, x_n, x_{n+1}), \tag{A2}$$

where $\theta(x, x_n, x_{n+1})$ must fulfill some conditions. It must be positive, defined and smooth and if x is far from the interval x_n, x_{n+1}, then $\theta(x, x_n, x_{n+1}) \to 0$. If we require continuous first derivatives of the smooth representation of the tabular data, it is straightforward to show that the first derivative of the weight function $\theta(x, x_n, x_{n+1})$ must also be continuous.

A natural way of fulfilling all these requirements is to define $\theta(x, x_n, x_{n+1})$ as

$$\theta(x, x_n, x_{n+1}) = \int_{x_n}^{x_{n+1}} w(x, x')\,{\rm d}x' \tag{A3}$$

with the exception of the first and the last intervals, for which

$$\begin{aligned} \theta(x, x_1, x_2) &= \int_{-\infty}^{x_2} w(x, x')\,{\rm d}x', \\ \theta(x, x_{N-1}, x_N) &= \int_{x_{N-1}}^{\infty} w(x, x')\,{\rm d}x' \end{aligned} \tag{A4}$$

where $w(x, x')$ is a function that must verify the normalization condition

$$\int_{-\infty}^{\infty} w(x, x')\,{\rm d}x' = 1. \tag{A5}$$

Note that $w(x, x')$ may be chosen in several ways. From a practical point of view, however, equation (A3) should be solvable analytically. The values of $y_\theta(x)$ obtained with our smoothing algorithm can be interpreted as the weighted sum of the contributions of each piece of the tabulated data.

It is important to note that with performing the smoothing in the way we propose, the resulting function does not pass exactly by the tabulated data. In the case where we choose $w(x, x') = \delta(x - x')$, where $\delta\,(x - x')$ is the Dirac function, integrating it in the corresponding interval we get the step function, which in turn makes us recover the original linear interpolation.

If the error in the linear interpolation is

$$e_n(x) = y(x) - y_n - y'_n(x - x_n) \tag{A6}$$

then, the error in the smooth representation $e_\theta(x)$ is

$$e_\theta(x) = \sum_{n=1}^{N-1} e_n(x)\,\theta(x, x_n, x_{n+1}). \tag{A7}$$

In the case that $\theta(x, x_n, x_{n+1})$ is chosen to be a narrow-peaked function around x, the error in the smooth representation should be comparable to that corresponding to standard linear interpolation. However, in the case where $\theta(x, x_n, x_{n+1})$ are not narrow-peaked, it seems difficult to give a useful bound to the error. Nevertheless, this case is of little interest, simply because the representation of the function would be too far from the original values.

A2 Some particular cases of weight functions

A possible choice for $w(x, x')$ is the rational function, which is

$$L_n(x - x') = C_n \frac{1}{[\Gamma^2 + (x - x')^2]^n}, \tag{A8}$$

with

$$C_n = \frac{(2n-2)!!}{(2n-3)!!}\,\frac{\Gamma^{2n-1}}{\pi}. \tag{A9}$$

This function is bell shaped, with its maximum at $x = x'$ and a characteristic width given by the free parameter Γ. As required, $L_n(x - x')$ has an analytical primitive. We will denote the integral as

$$\theta_n(x, x_j, x_{j+1}) \equiv \int_{x_j}^{x_{j+1}} L_n(x - x')\,\mathrm{d}x'. \tag{A10}$$

In spite of the fact that the analytic integral exists for arbitrary value of n, values of $n > 2$ will result in complicate expressions, expensive from a numerical point of view. Moreover, on studying the example proposed in Section A4 we found no obvious advantage in choosing $n = 3$. Thus, from here on, we shall concentrate on cases of $n = 1, 2$.

The expression for $y_{L_n}(x)$ is

$$\begin{aligned} y_{L_n}(x) = {} & [y_1 + y_1'(x - x_1)]\theta_n(x, -\infty, x_2) \\ & + \sum_{j=2}^{N-2} [y_j + y_j'(x - x_j)]\theta_n(x, x_j, x_{j+1}) \\ & + \left[y_{N-1} + y_{N-1}'(x - x_{N-1})\right]\theta_n(x, x_{N-1}, \infty). \end{aligned} \tag{A11}$$

In the case of $n = 1$ we have

$$\theta_1(x, x_j, x_{j+1}) = \frac{1}{\pi}\left[\arctan(U_j) - \arctan(U_{j+1})\right], \tag{A12}$$

whereas, in the case of $n = 2$ we have

$$\begin{aligned} \theta_2(x, x_j, x_{j+1}) = {} & \frac{1}{\pi}\left[\frac{U_j}{U_j^2 + 1} - \frac{U_{j+1}}{U_{j+1}^2 + 1}\right. \\ & \left. + \arctan(U_j) - \arctan(U_{j+1})\right]. \end{aligned} \tag{A13}$$

In the above expressions

$$U_j = \frac{x - x_j}{\Gamma}. \tag{A14}$$

A3 The spectrum of interpolation frequencies

The smoothing operation should only filter out those high frequencies present in the tabulated data which could make the convergence of the employed algorithms difficult. Otherwise, there is the risk of obtaining stable solutions that are very different (or even meaningless) from the true one. Thus, let us study the problem of the modification of the spectrum of frequencies of the linear interpolation when we apply the process of smoothing we propose in this Appendix. We shall adopt the definitions for the Fourier Transform and Antitransform as stated in, e.g. Duff & Naylor (1966)

$$F(s) = \frac{1}{\sqrt{2\pi}}\int_{-\infty}^{\infty} f(x)\,\mathrm{e}^{-isx}\,\mathrm{d}x, \tag{A15}$$

$$f(x) = \frac{1}{\sqrt{2\pi}}\int_{-\infty}^{\infty} F(s)\,\mathrm{e}^{isx}\,\mathrm{d}s. \tag{A16}$$

Applying these definitions to the algorithm presented in Section A2, the Fourier transform of the smooth representation can be written as

$$\begin{aligned} Y_\theta(s) = {} & \sum_{j=1}^{N-1}\left(y_j - y_j' x_j\right)\Theta(s, x_j, x_{j+1}) \\ & + i\sum_{j=1}^{N-1} y_j'\frac{\mathrm{d}}{\mathrm{d}}s\Theta(s, x_j, x_{j+1}), \end{aligned} \tag{A17}$$

where $\Theta(s, x_j, x_{j+1})$ is the Fourier transform of the weight function $\theta(x, x_j, x_{j+1})$ in the corresponding interval.

Now, let us study the particular case of the weight functions presented in Section A2. The Fourier transform of the weight function in this case is

$$\begin{aligned} \Theta_n(s, x_j, x_{j+1}) = {} & \frac{C_n}{\sqrt{2\pi}}\int_{x_{j+1}}^{x_j} \mathrm{d}x'\mathrm{e}^{-isx'} \\ & \times \int_{-\infty}^{\infty} \frac{\cos\left[s(x - x')\right]}{\left[\Gamma^2 + (x - x')^2\right]^n}\,\mathrm{d}(x - x'). \end{aligned} \tag{A18}$$

The last integral has a value that is independent of the interval. For the particular cases of $n = 1, 2$ their values are $\pi/\Gamma\exp(-s\Gamma)$ and $\pi/(2\Gamma^3)\ (1 + s\Gamma)\ \exp(-s\Gamma)$, respectively (see, e.g. Gradshteyn & Ryzhik 1994). Thus

$$\Theta_1(s, x_j, x_{j+1}) = \Theta_{\mathrm{step}}(s, x_j, x_{j+1})\exp(-s\Gamma) \tag{A19}$$

and

$$\Theta_2(s, x_j, x_{j+1}) = \Theta_1(s, x_j, x_{j+1})(1 + s\Gamma) \tag{A20}$$

where $\Theta_{\mathrm{step}}(s, x_j, x_{j+1})$ is the Fourier transform of the step function in this interval. It is clear that the smoothing of the linear interpolation acts as a lowpass band filter. Thus, for the cases of $n = 1, 2$ frequencies for which $\omega\Gamma \gtrsim 1$ are strongly damped.

A4 A numerical example

In this section we shall present an example of how our proposed algorithm works in the case of being employed to interpolate a definite function. For such a purpose, we have chosen the values of radiative opacities relevant for the physical conditions attained in the outer envelope of the giant planets (Guillot et al. 1994). In particular, the selected curve corresponds to element abundances corresponding to Jupiter at a density of $\rho = 10^{-14}$ g cm^{-3}. The curve is defined by 17 points that are unevenly spaced. The maximum and minimum intervals are 0.180 and 0.039, respectively.

To test the algorithm presented above, we shall employ the two weight functions considered in Section A2 for the cases $n = 1, 2$ assuming values of Γ similar to those corresponding to the table spacing.

We show in Fig. A1 the results of applying the algorithm we propose for the case of $n = 1$ for the data set cited above. In doing so we have assumed values for the free parameter Γ of $\Gamma = 0.03, 0.06, 0.12, 0.24$. The results presented in Fig. A1 clearly indicate that the method discussed in the present work is poor and not recommended for the case of $n = 1$. The overall behaviour of the method could be improved by restricting the interval of x but this would imply the introduction of highly undesirable boundary effects. Owing to this, we shall not consider the case of $n = 1$ any further.

Let us now consider the case $n = 2$. The results of the interpolation of the function are depicted in Fig. A2. From inspection of this figure it is quite clear that in this case the overall behaviour of the interpolation largely supersedes that corresponding to the case of $n = 1$. Only for the largest value of Γ there are some significative differences near the absolute minimum of the function.

For comparison, we have also included in such figures results corresponding to interpolation of the data at the same points as those performed with the Akima (1970) cubic spline algorithm which constructs a piecewise cubic polynomial curve close to a manually drawn curve. Note that for small values of Γ, that are comparable to the minimum spacing of the present data tabulation, our algorithm

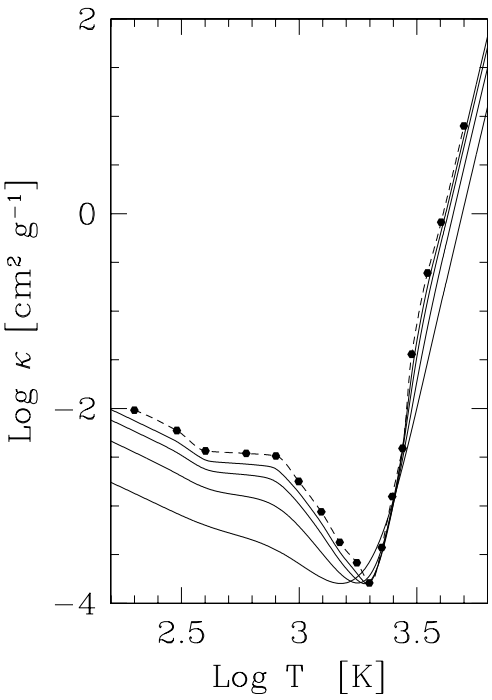

Figure A1. The interpolation of the opacity data values (represented by filled circles by means of the weight function defined by equation (A12) with values of $\Gamma = 0.03, 0.06, 0.12, 0.24$. The larger the Γ value, the worse the interpolated value. Also the results predicted by the Akima (1970) spline algorithm are included with short dashed lines. It is clear that the weight function equation (A12) provides a poor smoothed interpolation. This is so mainly as a result of its asymptotic behaviour (see text for more details).

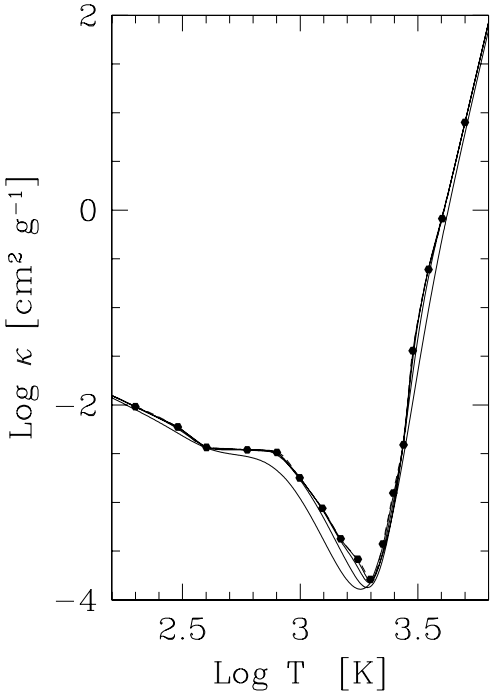

Figure A2. The interpolation of the opacity data values (represented by filled circles) by means of the weight function defined by equation (A13) for the same values of Γ as in Fig. A1. The larger the Γ value, the worse the interpolated value. The weight function equation (A13) provides a very good smoothed interpolation that, in the case of low Γ values is very similar to that given by the Akima spline algorithm (short dashed lines).

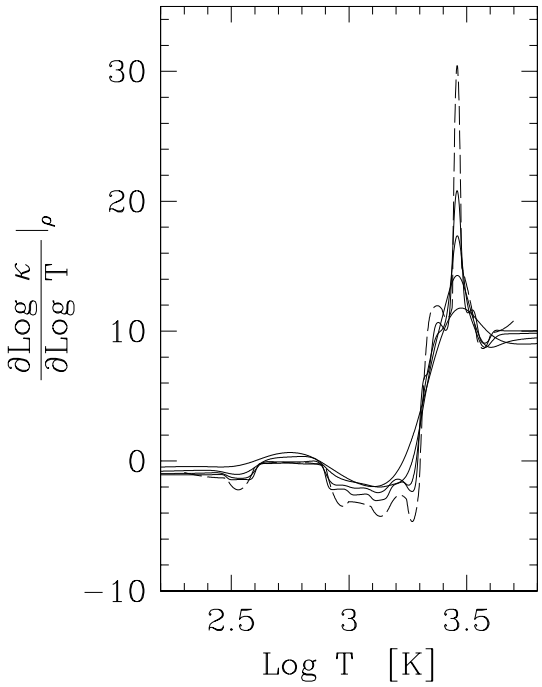

Figure A3. The derivative of the interpolation of the opacity data values assuming the weight function defined by equation (A13) for the same values of Γ together with the derivative given by the Akima spline interpolant. Notice that the Akima algorithm gives strongly oscillating derivatives.

with $n = 2$ produces results that are almost indistinguishable from those corresponding to the Akima spline.

In Fig. A3 we show the results corresponding to the derivative of the function for the case of $n = 2$ and the set of values of Γ employed in Figs A1 and A2 together with those given by the Akima spline. In spite of the fact that the Akima spline gives a fairly good interpolation as shown in Fig. A2, it is clear that it produces a derivative of the function that oscillates appreciably more than the one obtained with the smoothing here proposed, even for the smallest Γ values considered. This is, as discussed above, a highly desirable property for handling interpolation algorithms in iterative schemes.

A5 Some general remarks on the algorithm

In this Appendix we have presented a simple smoothed linear interpolation algorithm intended to represent tabulated functions. We presented a general treatment, and studied two particular cases in which we considered specific weight factors resulting from the integration of adequate rational functions in each interval of the tabulated data (see Section A2).

To test the performance of our algorithm, we have chosen a particular data set and computed interpolated values for different values of the free parameter Γ. We have found that, as expected, the results of the interpolation are closer to the original linear interpolation as $\Gamma \to 0$, while the function is smoother the larger Γ is. In the case of $n = 1$ the results are poor, while for $n = 2$ the algorithm works nicely when we assume that the Γ values are not larger than the data spacing. Moreover, our technique provides interpolated values very similar to those given by the Akima spline interpolation (Fig. A2) but with smoother derivatives. (Fig. A3).

As our main motivation in developing this algorithm was to have a reliable interpolation technique that was able to be employed as

a routine in implicit relaxation calculations, we see an interesting property of this technique as compared to that presented by Akima. Let us suppose that we are trying to solve a given system of equations by an iterative technique that fails to converge. Then, in the framework of this algorithm, we can, in principle adopt a very large Γ value that will provide a very inexact but smooth interpolation. After we get convergence we can compute a sequence of solutions of the iteration by lowering the Γ value in several steps. In such a way we can embed the initial artificial solution to produce a realistic solution. In the case of the Akima spline this is not possible, simply because there is no free parameter available to be handled in an equivalent way.

In addition, it should be noted that the algorithm presented in this Appendix can be straightforwardly generalized for representing multidimensional functions. This is so if we choose weight functions in separate variables.

This paper has been typeset from a TEX/LATEX file prepared by the author.